Aerosol Science & Technology

ISSN: 0278-6826 (Print) 1521-7388 (Online) Journal homepage: https://www.tandfonline.com/loi/uast20

Conditions for Cloud Settling and Rayleigh-Taylor Instability

William C. Hinds , Andre Ashley , Nola J. Kennedy & Paul Bucknam

To cite this article: William C. Hinds , Andre Ashley , Nola J. Kennedy & Paul Bucknam (2002) Conditions for Cloud Settling and Rayleigh-Taylor Instability, Aerosol Science & Technology, 36:12, 1128-1138, DOI: 10.1080/02786820290108449

To link to this article: https://doi.org/10.1080/02786820290108449

Aerosol Science and Technology 36: 1128–1138 (2002)

Published by Taylor and Francis
0278-6826/02/$12.00 + .00
DOI: 10.1080/0278682029010844 9

Conditions for Cloud Settling and Rayleigh-Taylor Instability

William C. Hinds,[1] Andre Ashley,[1] Nola J. Kennedy,[1] and Paul Bucknam[2]
[1]*Department of Environmental Health Sciences, Center for Occupational and Environmental Health, UCLA School of Public Health, Los Angeles, California*
[2]*Amerada Hess Corporation, Woodbridge, New Jersey*

Most aerosol motion can be analyzed by individual particle motion or by the motion of the suspending gas. There are, however, two related situations in which an aerosol can exhibit bulk motion: cloud settling and Rayleigh-Taylor instability. In both cases, the aerosol particles move faster as a cloud than they do as individual particles. In the case of cloud settling, the aerosol is usually a spheroidal cloud surrounded by clean air. Rayleigh-Taylor instability occurs when a dense aerosol layer overlies a layer of clean air. This instability is characterized by abrupt breakthrough of the aerosol layer into the clean air layer at multiple points. High-concentration, submicrometer test aerosols were generated in two experimental systems that permitted observation of the transition from particle-dominated motion to cloud, or bulk, dominated motion and measurement of cloud settling velocities and characteristics. In both systems aerosol concentration could be controlled over two orders of magnitude. One system used commercial ventilation smoke tubes to release a dense stream of aerosol into a low velocity wind tunnel. The other used diluted mainstream cigarette smoke from a smoking machine in an aerosol centrifuge. Based on these experiments, theoretical equations for cloud settling predict cloud settling velocity within an order of magnitude. The transition from individual particle motion to observable bulk motion occurs when predicted cloud settling velocity is from 0.01 to 0.05 m/s. Cloud settling appears to be initiated from an aerosol stream or layer by Rayleigh-Taylor instability. The ratio of cloud settling velocity to particle settling velocity does not appear to be a reliable predictor of the transition from particle to bulk motion.

INTRODUCTION

Most aerosol particle motion can be analyzed by the motion of the suspending gas or by individual particle motion due to settling, particle inertia, or Brownian motion. There are, however, two related situations in which an aerosol can exhibit bulk motion, cloud settling, and Rayleigh-Taylor instability. In both, the aerosol particles move faster as a cloud than they do as individual particles. A cloud is defined here as a region of high aerosol concentration with a well-defined boundary that is surrounded by a larger region of clean air. In the case of cloud settling the aerosol is usually a spheroidal-shaped cloud surrounded by clean air. Bulk motion can occur for aerosols with high concentration even when there is no difference in gas density between the suspending gas of the aerosol forming the cloud and that for the gas surrounding the cloud. The related phenomena of Rayleigh-Taylor instability occurs when a dense aerosol layer overlies a layer of clean air. This instability is characterized by abrupt breakthrough at multiple points of the aerosol layer into the clean air layer. The spacing between the breakthrough points and the relative rate of descent can be predicted from theory, see Plesset and Whipple (1974). Both require well-defined regions of clean air and aerosol and a difference in density between the aerosol and the clean air, either due to temperature, gas density, or high particle concentration. The effects can be quite dramatic. Prosad and Sen (1938) injected a stream of mainstream tobacco smoke into a glass chamber and observed a settling velocity of about 70 mm/s and incorrectly concluded that smoke particles had a mean size of 48 μm. Several other studies have concluded that tobacco smoke particles are submicrometer in size, see Hinds (1978).

The impetus for the present study began with an attempt to use commercial smoke tubes for flow visualization in a horizontal-flow, low-velocity wind tunnel. It was immediately apparent that the concentrated smoke stream was not following the air, but was settling as a cloud. This situation engendered the obvious question, at what concentration and stream size would the smoke move as individual submicrometer particles rather than as a cloud. A search of the experimental and theoretical literature on this subject provided little guidance. The theory, reviewed below, suggests that nearly every condition that would provide good flow visualization would also have significant cloud settling

Received 13 September 2001; accepted 25 March 2002.
This work was supported in part by United States NIOSH/DOE grant RO1/CCR912034 and NIOSH training grant T42/CCT918726.
Address correspondence to William C. Hinds, UCLA School of Public Health, 650 Young Drive South, Los Angeles, CA 90095-1772. E-mail: whinds@ucla.edu

motion. No published papers were found that gave guidelines as to the specific conditions when cloud settling or Rayleigh-Taylor instability would or would not occur. Consequently, the present study was undertaken to determine the conditions for which cloud settling or Rayleigh-Taylor instability can occur.

PREVIOUS WORK—CLOUD SETTLING

Fuchs (1964) and Hinds (1999) present the basic theoretical premise that whether or not cloud settling occurs depends on the ratio of the terminal settling velocity for a spherical cloud to that for the particles that make up the cloud. These authors provide little guidance as to when cloud settling will occur beyond stating that when the ratio is much greater than unity cloud settling occurs and when it is much less than unity it does not.

Stober et al. (1978), Chen and Yeh (1990), Martonen (1992), Phalen et al. (1994), and Robinson and Yu (2001) observed bulk motion of mainstream cigarette smoke in air. Martonen (1992) observed the path of mainstream smoke in human airway casts and concluded from theoretical analysis that cloud motion would occur when a 3 mm diameter cloud has a mass concentration much >52 mg/m^3. Chen and Yeh (1990) observed cloud settling of mainstream smoke in a glass tube and concluded that bounded clouds, clouds in a tube with no surrounding clean air, had settling velocities approximately half that predicted for unbounded clouds. Phalen et al. (1994) found enhanced deposition of mainstream cigarette smoke in hollow lung casts that they attributed to enhanced settling due to bulk motion. By assuming that the cloud settling was in the Stokes region they estimated the ratio of cloud settling velocity to particle settling velocity to be about 100.

Some investigators have approached the problem of cloud settling in terms of hydrodynamic interaction between particles due to their close spacing in concentrated clouds. These interactions allow the cloud to move faster as a cloud than as individual particles. It is known that two particles in close proximity will settle faster than the same particles far apart (Fuchs 1964; Wen 1996). For dense combustion clouds, with submicrometer-sized particles, the particles are at least 10 diameters apart and the particle-particle hydrodynamic interaction will increase settling velocity by $<10\%$. Because of the very low settling velocities of submicrometer particles, this effect cannot account for observed cloud settling.

PREVIOUS WORK—RAYLEIGH-TAYLOR INSTABILITY

The theory of Rayleigh-Taylor instability was first characterized by Taylor (1950) and confirmed experimentally by Lewis (1950). The instability exists in any two-fluid situation where a denser fluid layer overlies a less dense fluid in a gravitational or other type of force field. It is characterized by abrupt breakthrough of the denser layer into the less dense layer. Taylor's original characterization of the spacing of the breakthrough points and their rate of growth was improved upon by Plesset and Whipple (1974), who included the effect of fluid viscosity.

Hinds (1978) and Stober et al. (1978) observed bulk motion of aerosols consistent with Rayleigh-Taylor instability in aerosol centrifuges while measuring the size distribution of mainstream cigarette smoke. Both authors found that mainstream cigarette smoke had to be diluted 100:1 or more with clean air to prevent this instability. Interpretation of these results are complicated by the fact that the gas phase of undiluted cigarette smoke contains about 8% carbon dioxide and the centrifugal acceleration in their experiments ranged up to 1200 times that of gravity.

THEORY—CLOUD SETTLING

Cloud settling occurs when gravitational motion is much faster for a cloud, as an ensemble of particles moving together, than for individual particles. Consider a spherical cloud of diameter d_c and density ρ_c composed of monodisperse particles of diameter d_p and density ρ_p. The cloud can be considered a giant low density particle. The density of a cloud ρ_c is equal to the mass concentration of the particles in the cloud C_m plus the density of the suspending gas, the gas inside the cloud ρ_{cg}, or

$$\rho_c = C_m + \rho_{cg}. \qquad [1]$$

The settling velocity of a cloud, V_c, is obtained by equating the net downward force of gravity acting on the cloud to the drag force. Unlike particle settling, the buoyancy must be included when calculating cloud settling velocity. The general form for cloud settling velocity in terms of the drag coefficient C_D and Newton's drag equation (Hinds 1999) is

$$V_c = 1.1\left(\frac{4(\rho_c - \rho_a)d_c g}{3C_D\rho_a}\right)^{1/2}, \qquad [2]$$

where ρ_a is the density of particle-free air surrounding the cloud, g is the acceleration of gravity, and downward movement of the cloud is positive. The factor 1.1 accounts for reduced drag due to internal circulation within a cloud (Fuchs 1964). If the cloud density ρ_c is less than the density of the surrounding gas ρ_a, which it can be when the cloud gas is, for example, warmer than the surrounding gas, the cloud will rise rather than settle. C_D depends on the Reynolds number of cloud motion, $\mathrm{Re}_c = \rho_a V_c d_c/\eta$, where η is the viscosity surrounding gas.

For $\mathrm{Re}_c < 1$, cloud motion is in the Stokes region, $C_D = 24/\mathrm{Re}_c$, and Equation (2) becomes

$$V_c = 1.21\left(\frac{(\rho_c - \rho_a)d_c^2 g}{18\eta}\right) \quad \text{for } \mathrm{Re}_c < 1. \qquad [3]$$

For $1 < \mathrm{Re}_c < 1000$, V_c can be estimated by empirical equations given by Hinds (1999).

$$V_c = 1.1\left(\frac{\eta}{\rho_a d_c}\right)\exp(-3.070 + 0.9935J - 0.0178J^2), \qquad [4]$$

$$\text{where } J = \ln\left(\frac{4(\rho_c - \rho_a)\rho_a d_c^3 g}{3\eta^2}\right).$$

Table 1
Calculated cloud settling velocities for $\rho_{cg} = \rho_a$

Particle mass conc. (g/m^3)	Cloud settling velocity (m/s) [cloud Reynolds number]			
	$d_c = 1$ mm	$d_c = 10$ mm	$d_c = 100$ mm	$d_c = 1000$ mm
1.0	0.0000	0.0028	0.044	0.17
	[0.0024]	[1.8]	[290]	[11,500]
4.0	0.0001	0.0087	0.098	0.35
	[0.0097]	[5.8]	[650]	[23,000]
10.0	0.0004	0.018	0.17	0.55
	[0.024]	[12]	[1150]	[36,400]
40.0	0.0015	0.051	0.35	1.10
	[0.097]	[34]	[2300]	[72,800]
100.0	0.0036	0.097	0.55	1.73
	[0.24]	[65]	[3640]	[115,000]
400.0	0.015	0.25	1.10	3.46
	[0.97]	[163]	[7300]	[230,000]

When $10^3 < \mathrm{Re}_c < 10^5$, drag coefficient is approximately constant with a value of 0.44 and Equation (2) becomes

$$V_c = 1.91\left(\frac{(\rho_c - \rho_a)d_c g}{\rho_a}\right)^{1/2}. \quad [5]$$

Individual particle settling velocity, V_p, is given by Stokes law as

$$V_p = \frac{\rho_p d_p^2 C_C g}{18\eta}, \quad [6]$$

where C_C is the slip correction factor for a particle of diameter d_p.

The relative importance of the two settling mechanisms is given by the ratio of cloud settling velocity to particle settling velocity, G, as

$$G = \frac{V_c}{V_p}, \quad [7]$$

where V_c, the cloud settling velocity, is given by Equations (3)–(5) and V_p by Equation (6). When G is much greater than 1.0, cloud settling will predominate, and when G is much less than 1.0, individual particle motion will predominate.

The relationship between G and cloud size and cloud density varies with the cloud Reynolds number. In all cases, cloud settling velocity V_c and G increase with increasing $(\rho_c - \rho_a)$ and with increasing d_c. For $\mathrm{Re}_c < 1$, V_c and G are proportional to $(\rho_c - \rho_a)$ and to d_c^2. For $\mathrm{Re}_c > 1000$, V_c and G are proportional to $(\rho_c - \rho_a)^{1/2}$ and to $d_c^{1/2}$. For $1 < \mathrm{Re}_c < 1000$, the dependence of V_c and G on $(\rho_c - \rho_a)$ varies from 1 to $\frac{1}{2}$ power and on d_c varies from 2 to $\frac{1}{2}$ power as Re_c goes from 1 to 1000.

While the quantity G provides guidance as to the relative importance of cloud settling compared to particle settling, it is not very useful for predicting observable cloud settling for dense smokes. Smoke particles are submicrometer in size with settling velocities at usual ambient conditions on the order of 10^{-5} m/s. This is a low velocity and suggests that the value of G would have to be more than 1000 and probably more than 10,000 for the cloud settling velocity to be noticeable.

A more useful approach is to identify the conditions of mass concentration and cloud size that give a significant or observable cloud settling velocity, such as 0.01 m/s.

Note that Equations (3)–(5) are independent of particle properties, d_p and ρ_p. Table 1 gives calculated cloud settling velocities and cloud Reynolds numbers for specified mass concentrations C_m for monodisperse aerosol clouds of the indicated cloud size. Table 1 is limited to the condition where the suspending gas density ρ_{cg} equals the surrounding gas density ρ_a.

THEORY—RAYLEIGH-TAYLOR INSTABILITY

The related phenomena of Rayleigh-Taylor instability occurs when a dense aerosol layer is above a clean air layer. This instability is characterized by abrupt breakthrough of the aerosol into the clean air region at discrete points with periodic spacing. Spacing between breakthrough points, L, is given by Plesset and Whipple (1974):

$$L \cong 4.4\pi\left(\frac{2\eta^2}{\rho_a(\rho_c - \rho_a)g}\right)^{1/3} \quad [8]$$

for $\rho_c \gg \rho_a$ or $\rho_c \ll \rho_a$. For $\rho_c \gg \rho_a$, the downward plunging fingers develop very rapidly with a growth rate for an aerosol

layer that is thicker than approximately $L/3$ of

$$\text{Growth Rate} \propto \exp\left[\left(\frac{(\rho_c - \rho_a)\pi g}{\rho_a L}\right)^{1/2} t\right], \qquad [9]$$

where t is the time from the start of development (Plesset and Whipple 1974). In Equation (9) the rate is given in multiples of some initial perturbation that starts the process. Thus as aerosol concentration increases, the breakthroughs become somewhat more closely spaced and develop much faster. For both cloud settling and Rayleigh-Taylor instability, small differences between cloud density ρ_c and clean gas layer density ρ_a can have significant effects on bulk motion, whereas changes in air density have little effect on individual particle motion.

EXPERIMENTAL, WIND TUNNEL

Aerosol Generation

Ventilation smoke tubes (MSA Ventilation Smoke Tubes, p/n 458480, MSA, Inc., Pittsburgh, PA) were used to generate high-concentration aerosol streams. These tubes are used for flow visualization and ventilation studies. The smoke tubes produce a dense white cloud of polydisperse aerosol by passing air over pumice containing adsorbed stannic chloride. The stannic chloride reacts with moisture in the air, yielding an aerosol of tin oxides and hydrochloric acid. The smoke stream concentration gradually decreases with time as the stannic chloride is used up. For experiments conducted in the wind tunnel, the aerosol stream is delivered into the wind tunnel by a 6 mm inner diameter. Tygon tube at a constant flow rate of 0.2 L/min (Figure 1). The wind tunnel is described by Hinds and Kuo (1995). It is a large, low-velocity, open-cycle wind tunnel with a 1.6 × 1.6 m cross section. Room turbulence is removed by a layer of screen and a layer of honeycomb at the inlet. It was operated with a fixed horizontal velocity of 0.1 m/s.

Measurement of Mass Concentration

Measurement of the aerosol concentration was made by briefly collecting the entire output stream of the smoke tube onto 47 mm glass fiber filters. To minimize any sample bias the diameter, flow rate, and length of the sample line from the three-way valve to the filter was the same as that from the three-way valve to the smoke stream outlet in the wind tunnel. Concentration was calculated by measuring mass collected, smoke tube output flow rate, and sampling time. Due to the high concentrations, the samples were collected for 1 min periods to avoid overloading.

Measurement of Size Distribution

Size distribution of the smoke tube aerosol was measured using a Sierra Instruments Series 210 ambient cascade impactor. A portion of the smoke tube output flow was sampled with the cascade impactor. The mass collected on each stage was measured gravimetrically and used to determine the mass median diameter and geometric standard deviations for each of the 4 cloud settling conditions.

Observation of the Smoke Stream Path

The flowing smoke stream was observed through an acrylic window 0.7 m wide in the side of the wind tunnel. The smoke stream was observed by two observers and characterized into one of four levels of bulk motion: none, medium, heavy, and extra heavy. Descriptions of the four levels are given in the results section.

To make quantitative measurements of these plunging structures, the smoke stream was videotaped during the approximately 50 min lifetime of the smoke tube. The field of view was 0.7 m wide and 0.5 m high. The smoke stream was videotaped against a black background with a white grid (50 mm × 50 mm). The smoke stream was illuminated from above. The videotape was replayed and selected frames were captured to a personal computer with an All-In-Wonder Pro video board and

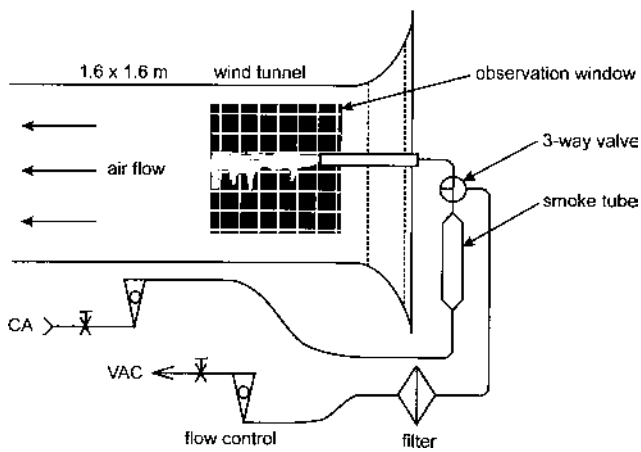

Figure 1. Schematic diagram of the wind tunnel experimental setup.

software (ATI Technologies, Inc., Thornhill, Ontario, Canada) at different time periods during a smoke tube's life corresponding to the four descriptive categories. During the capture period, captured frames were approximately 0.3 s apart and were printed out for measurement and analysis (see Figures 3a–c).

EXPERIMENTAL, AEROSOL CENTRIFUGE

A second set of data on cloud settling and Rayleigh-Taylor instability was obtained while measuring the particle size distribution of main stream tobacco smoke with a concentric aerosol centrifuge (Hinds 1978). In the centrifuge the aerosol enters the rectangular deposition channel at 80 cm^3/min as a 0.5 mm thick layer along the inner radius of the deposition channel. The annular deposition channel has a rectangular cross section 11 mm wide and 400 mm long and an inner radius of 60 mm. Clean air flows at 1.78 L/min in the remaining 10.5 mm of the channel width. Particles are centrifuged at about 660 times the acceleration of gravity. As a result of the centripetal force, they travel across the channel and deposit on a removable stainless steel foil lining the outer radius of the deposition channel. Large particles deposit near the inlet and small particles deposit farther along the channel. At the conclusion of sampling the foil is removed, cut into sections, each corresponding to a range of aerodynamic diameters, analyzed chemically for the collected particle mass, and from this the size distribution calculated.

Fresh mainstream tobacco smoke was generated with an automatic smoking machine using 85 mm nonfilter cigarettes. The machine has been described by Schultz and Wagner (1975). It holds 30 cigarettes and puffs each, once per minute, with a 35 cm^3 puff of 2 s duration to deliver a continuous stream of freshly-puffed smoke. The smoke can be diluted up to 20:1 prior to exiting the smoking machine. The smoke is delivered at atmospheric pressure. For experiments requiring more than 20:1 dilution, the smoke was further diluted by aspirating the smoke into a filtered air stream. The relative humidity of the dilution stream was approximately 20%. The smoke was presented to the centrifuge with dilutions ranging from 10:1 to 700:1, corresponding to aerosol concentrations of 11 and 0.16 g/m^3. The gas density of the undiluted tobacco smoke was calculated for the 18 most common gaseous components and found to be 1.228 kg/m^3. This can be compared to 1.204 kg/m^3 for clean air at 293 K. As a way to test for the presence of Rayleigh-Taylor instability, CO_2 was added to the carrier gas stream in different proportions to give this gas stream a density that could be adjusted from 1.205 to 1.38 kg/m^3.

RESULTS

Figure 2 shows average decay in output concentration for three smoke tubes at a constant flow rate through the smoke tube of 0.2 L/min. Over the 50 min life of the smoke tube the concentration decreases more then 150 fold from an initial concentration of more than 100 g/m^3. Also shown in the figure are the concentration ranges for the four levels of observed bulk motion.

The initial stream of smoke is significantly more dense than the surrounding air and quickly sinks several centimeters. Over approximately 50 min the concentration of smoke leaving the tube decreases gradually until no smoke can be seen leaving the outlet tube. The cloud settling phenomena is most pronounced at the beginning of the smoke tube output and decreases as the aerosol concentration decreases, becoming negligible during the last 15–20 min of smoke tube life.

The smoke stream appeared to have three regions as it moved through the first meter of the wind tunnel. The first region occurs immediately upon entering the wind tunnel, as the smoke exits the 6 mm Tygon tube. In this region the smoke enters the wind tunnel approximately isokinetically and moves with the air in the wind tunnel as a cohesive stream. This region is followed by an expansion region where the smoke stream enlarges and shows some turbulent motion. As the smoke stream grows it begins to exhibit the plunging behavior that is associated with Rayleigh-Taylor instability and cloud settling, the third region. This plunging behavior can be described as a series of inverted

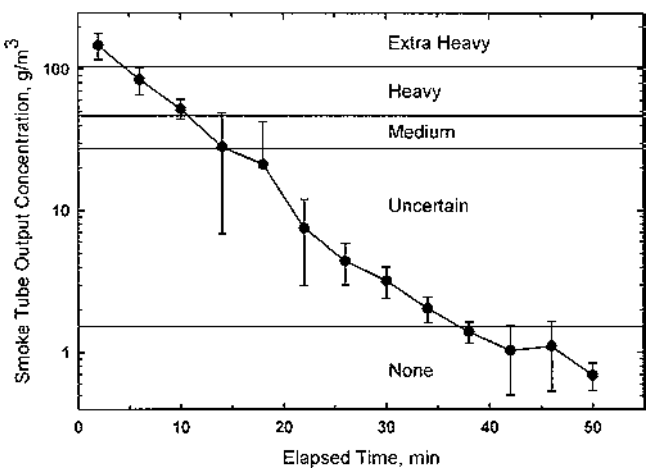

Figure 2. Decay in smoke tube output versus time. Average of 3 tubes. Error bars are $\pm 1\ \sigma$.

mushrooms emanating from the underside of the smoke stream. A finger of smoke about 20 mm in diameter forms at the bottom of the smoke stream and accelerates rapidly downward. These downward plunging fingers are believed to be a manifestation of Rayleigh-Taylor instability of the smoke stream. Once started the fingers partially detach and the cloud thus formed continues falling rapidly, leaving a wispy trail of smoke behind. After falling rapidly a few centimeters, the cloud spreads out laterally (horizontally) and its settling velocity slows significantly. This dropping and flattening cause the inverted mushroom shape described above. These plunging structures and the inverted mushrooms did not appear to rotate or spin. Occasionally during heavy bulk motion, one or two satellite or second generation plunging fingers descend from a flattened cloud. Satellite structures exhibit the same behavior as those descending from the main stream.

Four different levels of bulk motion were observed and characterized during the lifetime of each smoke tube. These were defined as extra heavy, heavy, medium, and none. The extra heavy condition is characterized by a rapid initial downward velocity of the entire smoke stream as it leaves the outlet. For this condition the smoke travels downward a few centimeters and then levels off as it expands and very quickly produces the characteristic inverted mushroom-shaped plunging structures. The extra heavy, heavy, and medium bulk motion conditions all produce the vertical plunging structures with lateral spreading and inverted mushroom shapes. However, the frequency and intensity of these structures differed among the three categories. The extra heavy condition rapidly forms many plunging structures due to its extremely high concentration. We observed more than 25 inverted mushroom structures at any instant over the 0.7 m observation range. The heavy and medium conditions also exhibit the inverted mushroom behavior, but it takes longer to develop the plunging structures and there are fewer of them, typically 15–25 and 5–15, respectively. The none condition is characterized by a barely visible smoke stream that does not form plunging aerosol clouds. It generally flows with a slight sinuous motion, but no plunging behavior. We were unable to make a clear distinction between medium and light and between light and none, so the light category was omitted.

Figures 3a–c are photographs of heavy, medium, and none bulk motion conditions. Identifiable plunging cloud structures are indicated by arrows. The elapsed time from the start of the experiment is shown in the upper left of each figure. The aerosol

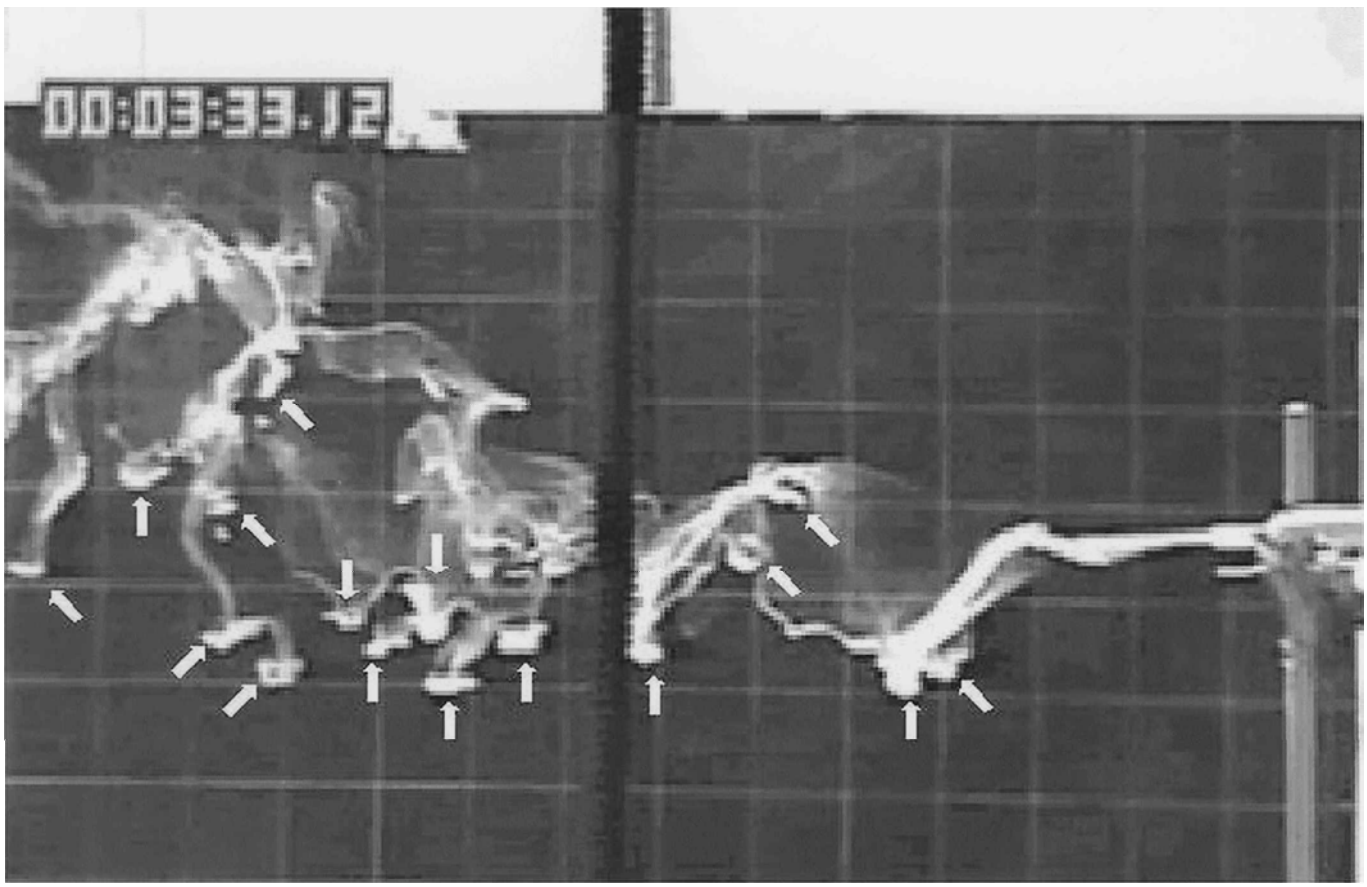

(a)

Figure 3. Photographs of smoke stream for (a) heavy condition, $C_m \cong 80$ g/m^3; (b) medium condition, $C_m \cong 30$ g/m^3; and (c) none condition, $C_m \cong 10$ g/m^3. Air motion is from right to left. *(Continued)*

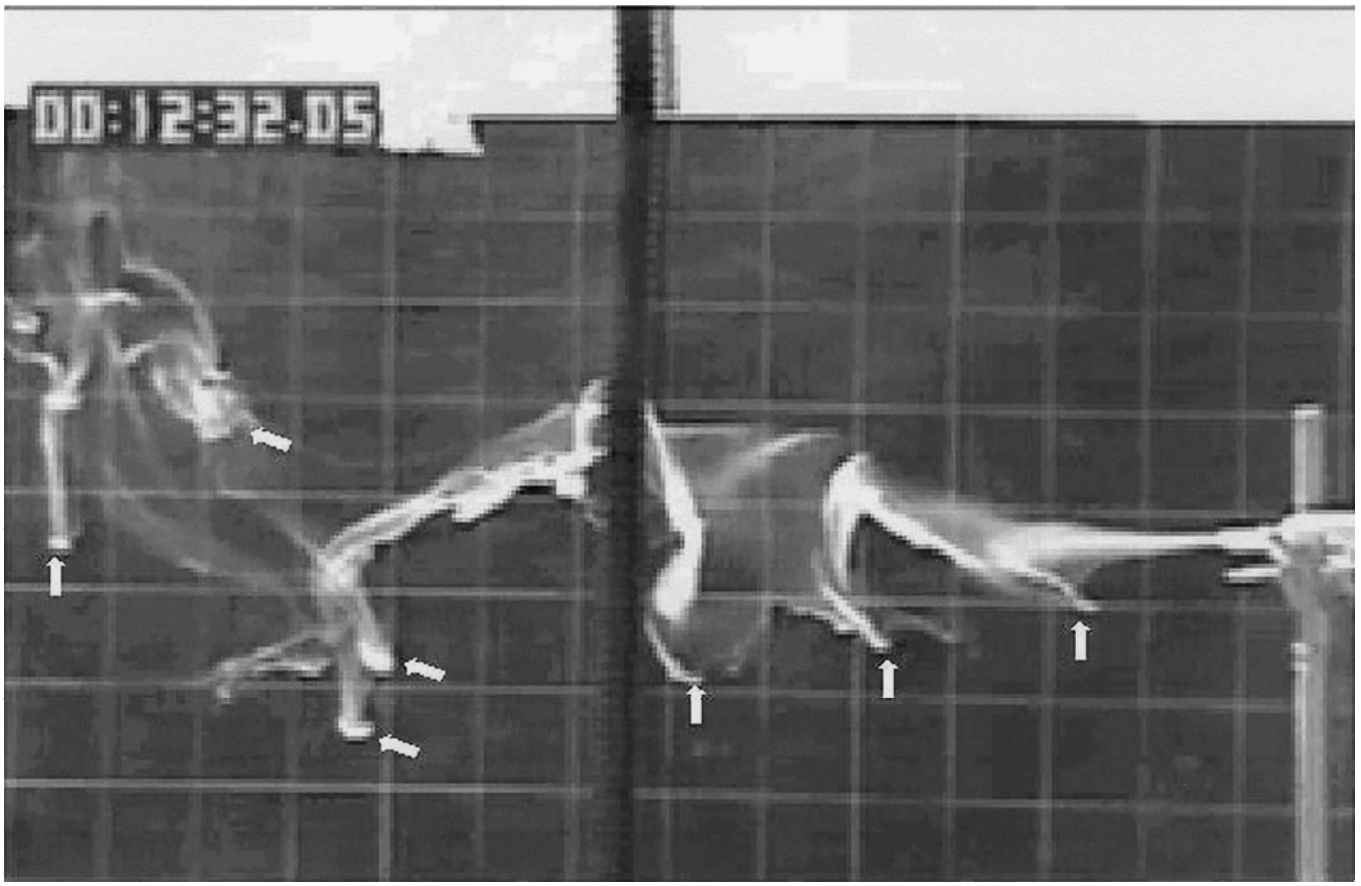

(b)

Figure 3. (Continued)

particle size distribution and stream dimensions and flow rate are the same for all three photographs, but the aerosol concentration ranges from 80 to 10 g/m^3 for Figures 3a–c.

Table 2 gives average aerosol properties for the four observed bulk motion conditions for the smoke tube experiments in the wind tunnel and for each of the mainstream tobacco smoke experiments in the concentric aerosol centrifuge. The average properties given are those at the time of observation or as close as could be measured. Number concentration is calculated from particle mass concentration and the diameter of average mass (obtained from the Mass Median Aerodynamic Diameter (MMAD) and geometric standard deviation (GSD) assuming a lognormal distribution; Hinds 1999). For these calculations the density of the gas inside the cloud ρ_{cg} was assumed to be equal to the density of the surrounding air ρ_a.

Table 3 presents the cloud settling and Rayleigh-Taylor instability data that were measured or estimated for each of the conditions given in Table 2. Measured and predicted cloud settling and Rayleigh-Taylor instability characteristics are compared in Table 4. Experimental cloud settling velocities were determined in two ways: average velocity over the entire observation period and average velocity during the active plunging period before the cloud flattens out and slows down. The latter were from 20–70% faster than those calculated for the entire observation period. Average velocity during active plunging was used in Tables 3 and 4.

Table 4 compares predicted cloud settling velocity for the observed bulk motions to measured bulk motion settling velocity. Values were calculated from data given in Table 2 and Equations (3)–(5).

Cloud spacing in the wind tunnel experiments was measured from video printouts and as such represent one-dimensional distances along the direction of airflow. The location of the actual structures varied in the direction perpendicular to the direction of the airflow (toward and away from the observer), so the measured cloud spacing represents minimum spacing. Table 4 compares predicted and measured spacing of the plunging structures for the wind tunnel experiments. Predicted spacing is based on Equation (8). The diameter of the settling clouds in the wind tunnel experiments was measured for 36 well-defined structures. Average results are given in Table 4.

Figure 4 compares all measured mass concentrations for the observed bulk motion conditions in the wind tunnel experiments. Error bars represent ± 2 standard errors of the mean.

Table 2
Properties of aerosols used

Observed bulk motion	Number of observations	Average particle mass concentration (g/m^3)	Calculated number concentration ($\#/cm^3$)	Acceleration (m/s^2)	MMAD (μm)	GSD
Smoke tube/wind tunnel						
None	7	8.1	1.1×10^9	9.8	0.74	2.64
Medium	7	33.5	1.0×10^9 (est)	9.8	–	–
Heavy	7	81.3	1.35×10^9	9.8	0.68	1.9
Extra heavy	1	123	5.3×10^8	9.8	1.38	2.15
Tobacco smoke/aerosol centrifuge						
None	1	0.16	3.4×10^6	6500	0.44	1.31
None	1	0.22	6.5×10^6	6500	0.46	1.35
None	1	0.34	1.0×10^7	6500	0.46	1.37
None	2	1.1	3.9×10^7	6500	0.44	1.38
Partial	2	2.2	6.5×10^7	6500	0.51	1.49
Unstable	3	5.5	7.4×10^7 (est)	6500	–	–
Unstable	3	11	1.1×10^8	6500	0.67	1.36

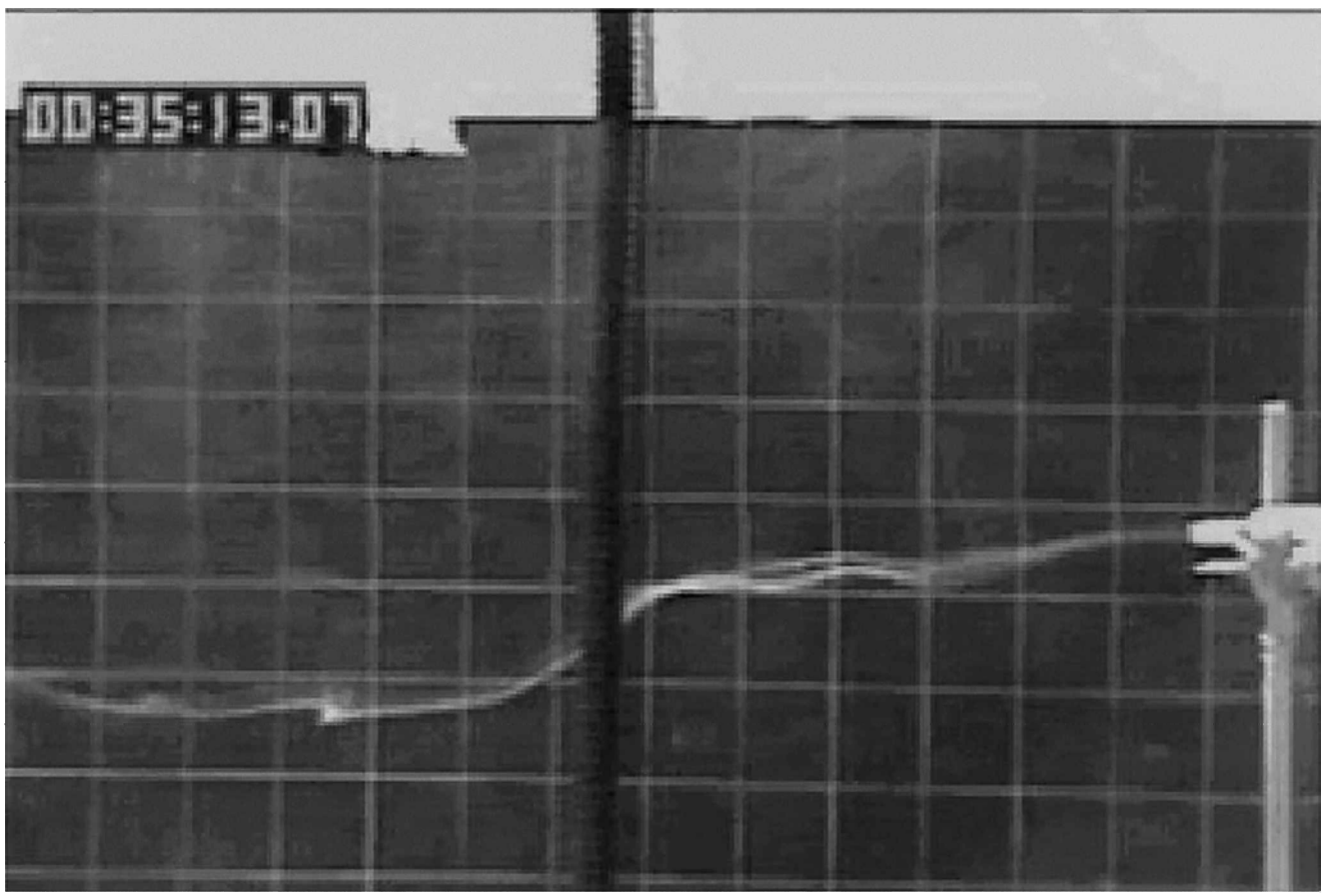

(c)

Figure 3. (Continued)

Table 3
Cloud settling and Rayleigh-Taylor instability data

Observed bulk motion	Particle mass concentration (g/m^3)	Average cloud diameter[a] (mm)	Measured settling velocity (m/s)	Cloud settling Reynolds number	Est. cloud spacing[b] (mm)	Cloud formation frequency (s^{-1})
Smoke tubes/wind tunnel (acceleration = 9.8 m/s^2)						
Medium	33.5	16	0.004	4.3	6.9	1.4
Heavy	81.3	16	0.021	22	3.5	2.9
Extra heavy	123	16	>0.021	>22	<2.8	>3.6
Tobacco smoke/aerosol centrifuge (acceleration = 6500 m/s^2)						
Partial	2.2	0.5	0.013	0.43	–	–
Unstable	5.5	0.5	0.025	0.82	–	–
Unstable	11	0.5	0.027	0.89	–	–

[a]Cloud diameter for smoke tube based on average horizontal dimension; for tobacco smoke based on stream width of 0.5 mm.
[b]Estimated average cloud spacing. Estimated by dividing the horizontal observation distance in the video images by the number of structures observed.

For the tobacco smoke experiments, the occurrence of instability was determined by observation of anomalous particle deposit on the deposition foil. In the absence of instability, the deposit was smoothly graded over the foil length corresponding to a lognormal distribution with a GSD of approximately 1.35. When instability occurred, the deposition was confined to a narrow region, a few centimeters from the inlet, and nowhere else. The difference in appearance is striking, and it is immediately apparent that this is an anomalous deposition pattern. The instability was an all-or-nothing phenomena in all except 3 of 27 tests conducted. In these three cases the results were intermediate with characteristics of both types of deposition.

Depending on the smoke dilution, the cloud density for the cigarette smoke stream ranged from 1.205 to 1.31 kg/m^3. The carrier gas stream could be adjusted over a similar range by the addition of CO_2. Instability was observed in 7 tests where the carrier gas density was less than <1.01 times the cloud density. Instability was not observed in 17 tests where the carrier gas density was >1.05 times the cloud density. For the three tests where the results were ambiguous, the carrier gas density ranged from 2 to 3% greater than the cloud density. This suppression effect occurs even though molecular diffusion would be expected to equalize the gas density differences within 0.5 s.

Table 4
Comparison of predicted and measured bulk motion

Observed bulk motion	Particle mass concentration (g/m^3)	Cloud settling velocity (m/s)			Ratio G based on		Cloud spacing (mm)	
		Measured	Predicted	Ratio meas./pred	Measured velocity	Predicted velocity	Measured	Predicted
Smoke tubes/wind tunnel (acceleration = 9.8 m/s^2)								
None	8.1	–	0.026	–	–	1290	–	–
Medium	33.5	0.004	0.071	0.056	1190	3810	6.9	15
Heavy	81.3	0.021	0.17	0.12	1110	10200	3.5	11
Extra heavy	123	>0.021	0.22	>0.10	300	3520	2.8	9.6
Tobacco smoke/aerosol centrifuge (acceleration = 6500 m/s^2)								
None	0.16	–	0.0009	–	–	0.17	–	–
None	0.22	–	0.0012	–	–	0.21	–	–
None	0.34	–	0.0019	–	–	0.33	–	–
None	1.1	–	0.006	–	–	1.14	–	–
Partial	2.2	0.013	0.012	1.0	1.92	1.77	–	–
Unstable	5.5	0.025	0.030	0.76	2.77	3.32	–	–
Unstable	11	0.027	0.051	0.53	2.45	4.61	–	–

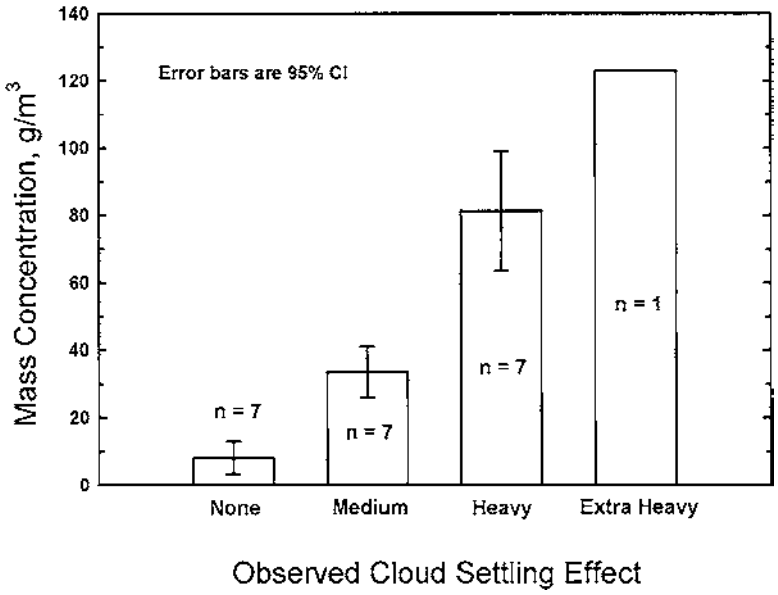

Figure 4. Mass concentration for the 4 observed conditions of bulk motion. Average of 7 runs. Error bars are $\pm 1\sigma$.

DISCUSSION

Bulk motion was observed for high concentration aerosols in two quite different physical situations. In both, bulk motion was observed at the highest concentrations and was not observed at the lowest concentrations. The transition from particle to bulk motion for each situation is internally consistent, but in comparing them they differ by a factor of more than 1,000 in predicted value of G for the transition from particle to bulk motion. As shown in Table 4, the transition for the smoke tube experiments occurs at about $G \cong 2000$, whereas it occurs at about $G \cong 1.5$ for the tobacco smoke/centrifuge experiments. This suggests there are other factors, not included in G, that affect this process.

The predicted cloud settling velocities for the range of conditions given in Table 4 vary by a factor of more than 200. The particle settling velocities for the particle sizes used in these experiments, and given in Table 2, vary by only a factor of 8. Consequently, the values of G, the ratio of cloud to particle settling velocity, shown in Table 4 cover a wide range that primarily reflects the cloud settling velocities rather than the differences in particle settling velocities. Furthermore, because particle settling velocities for submicrometer particles are very low, G may vary over a wide range and still be associated with negligible cloud settling velocities. This problem does not occur when using the predicted cloud settling velocity itself to estimate the transition from particle motion to cloud motion. For these experiments, predicted cloud settling velocity agrees within a factor of 10–18 with measured cloud settling velocities (see Table 4). Thus using the condition of predicted cloud settling velocity exceeding a value determined to be significant for the particular system provides a more robust prediction for the transition from particle to bulk motion.

The Reynolds numbers for cloud settling for the range of conditions given in Table 1 range from 0.002 to 230,000, a range that includes cloud motion in the Stokes, transition, and Newtons drag regions. This complicates the interpretation of the role of the different variables because different drag equations are used for each region.

As shown in Table 2, the calculated number concentration for these experimental conditions ranges from 10^6 to $10^9/\text{cm}^3$, a range for which coagulation can be slow or fast compared to the time scales for observation. At the highest number concentration coagulation is reducing number concentration and increasing average particle size rapidly. This is also the concentration range where bulk motion is most likely to occur. An examination of Equations (3)–(5) reveals that the effect of an increase in particle size due to coagulation is to decrease the value of G and thus the likelihood of bulk motion with time. This may limit the duration of bulk motion. Coagulation does not affect the value of predicted cloud settling velocity.

It is difficult to create aerosols with high mass concentration except in two circumstances: (1) aerosols created by combustion or gas-phase chemical reactions that have high number concentrations and submicrometer particle sizes, and (2) coarse solid particles that are fluidized for pneumatic transport or other similar activities. In the latter case the particles are solid with particle sizes mostly >20 μm, so their particle settling velocities are already quite high and cloud motion might go unnoticed.

Measured and predicted cloud settling velocities showed the same trend and agreed within a factor of 10 to 18 for the wind tunnel experiments and 1 to 2 for the aerosol centrifuge experiments. Given the complexity of this process and the difficulty of observation, this seems to be a reasonable agreement. Although the clouds for heavy and medium conditions are the same size, the average cloud settling velocity for the heavy condition is about 5 times greater than for the medium condition. This is

believed to be a result of the greater driving force due to the 2–3 times greater cloud density.

Measured and predicted spacing of the plunging structures in the wind tunnel experiments show the same trend and agree within a factor of 3 with each other. This supports the idea that the initial formation of the plunging clouds is controlled by Rayleigh-Taylor instability of the smoke stream.

In the wind tunnel experiments the measured diameter of 36 well-defined clouds showed no difference between those for heavy and medium conditions, so the overall average value is given in Table 3 and was used for subsequent calculations. The clouds were not spherical, but showed some horizontal flattening with heights about 70% of widths. Cloud diameters were estimated by comparing equivalent projected area diameters shown on the video printouts to standard circles of known area.

To summarize the similarities, both cloud settling and Rayleigh-Taylor instability require an aerosol region and a clean air region. For downward motion, both require cloud density to be greater than clean air density, $\rho_c > \rho_a$. This can be due to greater gas density inside the cloud ρ_{cg}, high particle mass concentration C_m, or both.

Cloud settling differs from Rayleigh-Taylor instability in that it requires the cloud to be reasonably compact, usually spheroidal, and surrounded by clean air. Rayleigh-Taylor instability requires the aerosol to be in the form of a horizontal layer or stream with the clean air below it. The breakthrough points have the form of plunging cylinders or sheets of aerosol. Some characteristics of the breakthrough depend on the thickness of the aerosol layer. Cloud settling occurs where the clouds are formed or introduced, but breakthrough points of Rayleigh-Taylor instability occur periodically along the layer. Both may occur together or cloud settling may be initiated by Rayleigh-Taylor instability, which is followed by breakup of the plunging stream into discrete clouds that exhibit cloud settling.

Theoretically, the two phenomena can be distinguished by the velocity of fall. The settling velocity of a cloud quickly reaches its predicted terminal settling velocity, Equations (3)–(5), whereas the plunging instabilities proceed with increasing acceleration as long as the fall distance is smaller than the layer thickness (Plesset and Whipple 1974). The difference in density between the cloud and the clean air region ($\rho_c - \rho_a$) affects cloud settling velocity as the 0.5 or 1.0 power ($V_{TS} \propto \rho_c^{0.5}$, $V_{TS} \propto \rho_c^{1.0}$), but it affects the rate of development of Rayleigh-Taylor instability as the exponential of the 0.5 power (Rate $\propto \exp(\rho_c^{0.5})$.

For cloud settling with Re > 10,000, a comparison of terminal settling velocities could be misleading because it may take seconds or longer for such a cloud to reach its terminal settling velocity. For such conditions the distance traveled in 1 s would be a more appropriate measure for comparison. However, during their acceleration, erosion, coagulation, and dilution would change the properties of the cloud to reduce the cloud settling effect. All the clouds studied here were calculated to reach 95% of their terminal settling velocity in <0.1 s, so terminal settling velocity was used for comparison.

From Table 4 the predicted cloud settling velocity for the transition from individual particle motion to bulk motion occurs at about 0.05 m/s for the smoke tube experiments and at about 0.01 m/s for the tobacco smoke experiments. In the opinion of the authors, this is a useful way of identifying the transition from individual particle to bulk motion.

CONCLUSION

Based on these experiments the transition from individual particle motion to observable bulk motion occurs when predicted cloud settling velocity is from 0.01 to 0.05 m/s. Cloud settling appears to be initiated from a horizontal aerosol stream or layer by Rayleigh-Taylor instability. Cloud settling velocity can be predicted within an order of magnitude by the methods outlined here. The velocity ratio G does not appear to be a reliable predictor of the transition from particle to bulk motion.

REFERENCES

Chen, B. T., and Yeh, H. C. (1990). Effects of Cloud Behavior on a Cigarette Smoke Aerosol, *Lovelace Foundation Report LMF-129*, Albuquerque, NM.

Fuchs, N. A. (1964). *The Mechanics of Aerosols*, Pergamon Press, Oxford, UK.

Hinds, W. C. (1978). Size Characteristics of Cigarette Smoke, *Am. Ind. Hyg. Assoc. J.* 39:48–54.

Hinds, W. C. (1999). *Aerosol Technology*, 2nd Ed., John Wiley & Sons, New York.

Hinds, W. C., and Kuo, T. L. (1995). A Low-Velocity Wind Tunnel to Evaluate Inhalability and Sampler Performance for Large Dust Particles, *Appl. Occup. Environ. Hyg.* 10:549–556.

Lewis, D. J. (1950). The Instability of Liquid Surfaces when Accelerated in a Direction Perpendicular to their Planes, II., *Proc. Ro. Soc. Lond. A* 202:81.

Martonen, T. B. (1992). Deposition Patterns of Cigarette Smoke in Human Airways, *Am. Ind. Hyg. Assoc. J.* 53:6–18.

Phalen, R. F., Oldham, M. J., Mannix, R. C., and Shum, G. M. (1994). Cigarette Smoke Deposition in the Tracheobronchial Tree: Evidence for Colligative Effects, *Aerosol Sci. Technol.* 20:215–226.

Plesset, M. S., and Whipple, C. G. (1974). Viscous Effect in Rayleigh-Taylor Instability, *Physics of Fluids* 17:1–7.

Prosad, K., and Sen, D. N. (1938). On the Trajectory of Ash Particles in Air and the Determination of their Size, *Philosophical Magazine* 25:993–1008.

Robinson, R. J., and Yu, C. P. (2001). Deposition of Cigarette Smoke Particles in the Human Respiratory Tract, *Aerosol Sci. Technol.* 34:202–215.

Schultz, F. J., and Wagner, J. R. (1975). A Thirty Port Smoking Machine for Continuous Smoke Generation, *Beitrage zur Tobakforshung* 8:53–59.

Stober, W., Martonen, T. B., and Osborne, S. (1978). On the Limitation of Aerodynamical Size Separation of Dense Aerosols with the Spiral Duct Centrifuge. In *Recent Developments in Aerosol Science*, Chap. 12, edited by D. T. Shaw. John Wiley & Sons, New York.

Taylor, G. I. (1950). The Instability of Liquid Surfaces when Accelerated in a Direction Perpendicular to their Planes, I, *Proc. Royal Soc. Lond. A* 201:192–196.

Wen, C. S. (1996). *The Fundamentals of Aerosol Science*, World Scientific, Singapore.